Malaysian Journal Of Civil Engineering

Full Paper

A NUMERICAL STUDY OF THE EFFECT OF GROUND MOTIONS AND GAP DISTANCE DUE TO SEISMIC POUNDING WITH THE USE OF GAP ELEMENT BETWEEN REGULAR AND IRREGULAR ADJACENT STRUCTURES

Azmain Azad, Rakibul Hasan Abid, Md Imtiaz Nibir, Fatema-Tuz-Zahura*

Department of Civil Engineering, Ahsanullah University of Science and Technology, Dhaka, Bangladesh

*Corresponding author
fatema.edu@aust.edu

Article history
Received
26 October 2024
Received in revised form
06 May 2025
Accepted
06 May 2025
Published online
31 July 2025

Graphical abstract

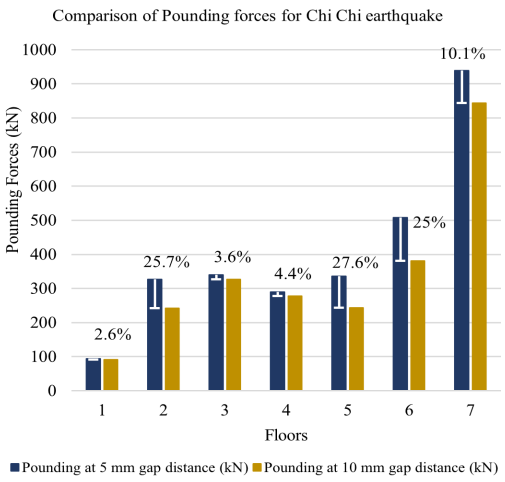

Abstract

Earthquakes with high magnitudes and strong ground motion have a more pronounced impact on structures that are positioned in close proximity to one another, as opposed to those that are more widely spaced. This proximity can lead to structural pounding, resulting in significant damage or even localized failure. The extent of pounding is influenced by both the insufficient separation distance between adjacent structures and the intensity of ground motion. Building codes worldwide stipulate a minimum separation distance to mitigate these effects. This study aims to evaluate the seismic pounding forces between adjacent reinforced concrete structures under varying ground motions, and to assess the influence of separation distance and structural irregularity on pounding behavior. Additionally, the effect of the structural mass on pounding force has also been discussed. Adjacent structures with differing floor levels were considered, and non-linear time history analyses were conducted using finite element-based software. Four real earthquake records with diverse characteristics and magnitudes were used to simulate ground motion effects. The results demonstrate that both Peak Ground Acceleration (PGA) and separation distance significantly affect the magnitude of pounding forces. Specifically, higher PGA values lead to substantial variations in pounding forces across different floors, while increased separation distance reduces the impact of pounding forces between adjacent structures. Moreover, structural irregularity and structural mass also contributes to differentiating the pounding forces.

Keywords: Seismic Pounding, Ground Acceleration, Gap Distance, Adjacent Structures, ETABS.

1.0 INTRODUCTION

Seismic pounding, also known as the "Pounding Effect," occurs when adjacent buildings with distinct dynamic characteristics collide during seismic events. This phenomenon poses significant risks to the structural integrity of the affected buildings and the safety of their occupants, potentially leading to substantial damage. Understanding the causes, characteristics, and consequences of seismic pounding is crucial for engineers, architects, and urban planners to design safer and more resilient structures in earthquake-prone areas. The collisions during seismic pounding can generate high forces and stresses that surpass the designed capacities of structural elements. This can result in various types of damage, including cracks in walls, columns, and beams, deformation of structural elements, and potentially partial or total collapse of the buildings. Pounding-induced damage can compromise the structural integrity of individual buildings, diminishing their seismic resilience and increasing vulnerability to future seismic events. Furthermore, the cumulative effects of pounding can propagate through interconnected structures, causing extensive damage and disruption in urban areas. To enhance the resilience of structures in earthquake-prone regions, effective design strategies and risk mitigation measures must take into account the factors influencing the frequency and intensity of seismic pounding. Addressing the challenges posed by seismic pounding necessitates advancements in seismic engineering and urban planning to ensure the stability and safety of our built environment in the face of seismic hazards. Ground motion is also a significant phenomenon in earthquakes and it influences the pounding effect as well. Ground motion in an earthquake refers to the movement of the earth's surface resulting from seismic waves generated by the sudden release of energy in the Earth's crust. This phenomenon is characterized by complex vibrational patterns that propagate through geological materials. The frequency of ground motion affects structural responses, where lower frequencies lead to prolonged oscillations and higher frequencies cause rapid vibrations. The duration of shaking, ranging from brief to extended, also influences structural impacts. Localized variations can create "hot spots" of intensified shaking. Understanding these factors is essential for seismic risk assessment, designing earthquake-resistant structures, and developing mitigation strategies to enhance community resilience in seismic areas. Nonlinear time history analysis is conducted to analyze the pounding effects and resilience of adjacent structures during earthquakes. The process of time history analysis involves breaking down the time domain into small intervals and employing numerical integration techniques to solve the equations of motion at each interval. This facilitates the observation of structural responses over time, incorporating the dynamic interactions among different structural elements and the evolving characteristics of ground motion. This enables engineers to precisely evaluate structural performance, identify potential failure modes, and devise appropriate retrofitting strategies to enhance structural resilience and mitigate seismic risks by considering nonlinear effects. Over the series of studies between 1986 and the current date, incremental understanding of the effects of structural pounding during earthquakes has been made. In their initial studies of 1986, Rosenbluth and Meli (Meli and Rosenblueth 1986) established that structural pounding was responsible for 40% of earthquake damage during the Mexico earthquake; damage due to pounding was significantly higher than that which resulted from structural collapses. In the studies that followed, Anagnostopoulos and Spiliopoulos in 1992 (Anagnostopoulos and Spiliopoulos 1992), among others, Papadrakakis and Mouzakis in 1995 (Papadrakakis and Mouzakis 1995) identified that numerical simulations play an important part in the study of dynamic responses of buildings in seismic events specifically and noted that pounding produced amplitude displacement. In 1997, Kasai and Maison (Kasai and Maison 1997) investigated the Loma Prieta earthquake, discovering over 200 cases of pounding damage across more than 500 buildings situated within 90 km of the epicenter. Their findings underscore the potential for significant damage in future seismic events. Further upgraded researches like Jeng and Tzeng (Jeng and Tzeng 2000) highlighted vulnerabilities in urban structures due to misaligned buildings. Jankowski in 2009 (Jankowski 2009) found that heavier buildings experience increased pounding damage, while his 2010 (Jankowski 2010) study differentiated effects on flexible and rigid structures. Cole in 2012 (Cole, Dhakal, and Turner 2012), categorized buildings susceptible to pounding, emphasizing the importance of adequate seismic separation gaps. In 2007, Favvata (Favvata 2017) determined the minimum gap required to prevent pounding in adjacent buildings with unequal story heights. Abdel Raheem's extensive work (2006-2018) (Raheem 2006, 2009; Abdel Raheem and Hayashikawa 2013; Raheem 2013a; Raheem 2013b; Abdel Raheem 2014; Abdel Raheem et al. 2018) categorized building types and analyzed pounding effects, noting significant damage in series of adjacent structures during earthquakes. Despite these insights, there is a lack of comparative research on high-rise versus low-rise buildings and irregularly shaped structures under varying ground motions. This study aims to address the gap distance by investigating how adjacent high-rise and low-rise buildings of regular and irregular shapes respond to different seismic activities. Figure 1 is the example of how adjacent structures stand nearby, where Figures 2 and 3 illustrate the way they collapse due to the strike of earthquake.

Figure 1 Types of adjacent structures. (Kazemi, Miari, and Jankowski 2021)

Figure 2 Collapse patterns of adjacent structures. (Rai et al. 2016)

Figure 3 Collapse patterns of adjacent structures. (Patil, Biradar, and Doddamani 2022)

2.0 METHODOLOGY

2.1 Different Pounding Models

In this article, there are brief descriptions about the models that have been used to simulate collisions between neighboring buildings during seismic events, focusing on the importance of building distance, model types like the stereo mechanical model and linear spring model, Kelvin-Voight element model and enhancing model accuracy and predictive power to improve urban infrastructure resilience.

The stereo mechanical model, first simulated by Goldsmith and Frasier (Goldsmith 1999), calculates the final velocity of colliding bodies using initial velocities and material properties via the coefficient of restitution. This coefficient, determined experimentally by measuring the rebound height of a dropped sphere, ranges from 0 (plastic collision with energy loss) to 1 (elastic collision with no energy loss). However, the model's limitations in handling systems with multiple degrees of freedom and collisions highlight the need for more adaptable techniques. Consequently, advanced computer simulations are being developed to predict and evaluate structures under simultaneous impact scenarios, crucial for designing safer, more resilient structures, especially in earthquake-prone regions. Equation (3) shows how to get the coefficient of restitution, which has been used to calculate the velocities of the colliding model after the impact in equation (1) and (2).

$$\upsilon'1 = \upsilon1 - (1 + e)\frac{m_2\ (v1-v2)}{m_1+m_2} \quad (1)$$

$$\upsilon'2 = \upsilon2 - (1 + e)\frac{m_2\ (v1-v2)}{m_1+m_2} \quad (2)$$

$$e^2 = \frac{h*}{h} \quad (3)$$

Where,
υ1= Velocity of colliding model m1 before impact;
υ2= Velocity of colliding model m2 before impact.
υ'1= Velocity of colliding body m1 after impact;
υ'2= Velocity of the colliding body m2 after impact;
e= The coefficient of restitution.

Maison and Kasai (Maison and Kasai 1990) used the linear elastic spring model to depict the contact element, also known as the gap element, between neighboring buildings. The axial stiffness of the components inside the in-contact structures serves as the basis for the stiffness of this model. By considering the neighboring structures as masses (m1 and m2) the linear spring model has been illustrated in Figure 4. Here, the buildings' relative velocity modifies the displacement between them as they vibrate out of time. Once the actual displacement between the structures is more than the initial gap that is specified, the spring begins to absorb forces. Equations (4) and (5) provide formulas for quantifying the forces (Fc) applied to the contact or gap element.

$$Fc = k_1\,(u_1 - u_2 - g_p); \qquad u_1 - u_2 - g_p \geq 0 \quad (4)$$

$$Fc = 0; \qquad u_1 - u_2 - g_p < 0 \quad (5)$$

Where, u_1 & u_2 = displacements of the impacting masses during oscillation;
k_1 = The spring stiffness constant;
g_p = The initial separation distance between the structures.

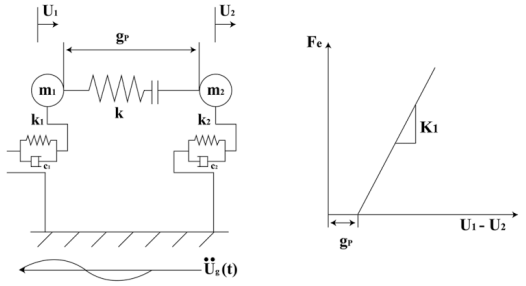

Figure 4 Linear spring model between two masses. (Kamel 2023)

One of the main improvements in Kelvin-Voight element model, as seen in Figure 5, is the addition of a damper that runs in parallel with a linear spring. The reason this damper is so important is that it dissipates energy, an idea that Anagnostopoulos employed back in 1988 (Anagnostopoulos 1988). By regulating the dynamic responses to outside forces, the damper improves the overall stability and efficiency of the model in addition to helping to lower the total vibrational energy inside the system. Improved performance and dependability are now possible in real-world applications where energy dissipation is crucial thanks to this breakthrough.

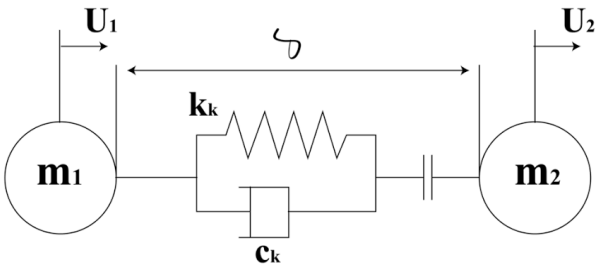

Figure 5 Kelvin-Voight element (Ghosh and Kumar 2023)

The second term, energy dissipation during mass vibration is taken into consideration by the expressed equations (6) and (7)

$$F_c = k_k(u_1 - u_2 - g_p) + c_k(u_1' - u_2');$$

$$when\ u_1 - u_2 - g_p \geq 0 \quad (6)$$

$$F_c = 0\ ; when\ u_1 - u_2 - g_p < 0 \quad (7)$$

Where u_1, u_2= Its derivatives are the displacements and velocities of the impacting bodies;

k_k= The spring constant of the element;

g_p= The initial separation distance between the structures.

The damping coefficient can be related to the damping ratio(ζ) which is related to the coefficient of restitution (e) that is expressed by equations. (8) and (9)

$$C = 2\zeta\sqrt{K\frac{m_1 m_2}{m_1+m_2}} \quad (8)$$

$$\zeta = \frac{-ln(e)}{\sqrt{\pi^2 + \ln(e)^2}} \quad (9)$$

To analytically obtain the pounding force in spring it must be added to the general equation of motion (Ks) have been expressed by equation (10).

$$m\ddot{x} + c\dot{x} + kx + ks\,x = m\ddot{g} \quad (10)$$

Where, for all degrees of freedom,

x= The displacement vector;

ẋ= The velocity vector;

ẍ= The acceleration vector.

m= The mass matrix;

c= The damping matrix estimated by the Rayleigh Equation;

k= The stiffness matrix for the structure's degrees of freedom.

ẍg= The input ground motion;

ks= The stiffness matrix for the gap element.

When colliding occurs between two structures each of them estimated by equation (11) and (12) according to the gap element under compression or tension force as shown in Figure 6.

$$m_1\ddot{x}_1 + c_1\ddot{x}_1 + k_1x_1 + k_sx_1 = -m_1\ddot{x}_g \quad (11)$$

$$m_2\ddot{x}_2 + c_2\dot{x}_2 + k_2x_2 - k_sx_2 = -m_2\ddot{x}_g \quad (12)$$

Where x_1 and its derivatives $\dot{x}_1$ and $\ddot{x}_1$ are displacement, velocity, and acceleration for structure (1) respectively while x_2 and it derivatives $\dot{x}_2$ and $\ddot{x}_2$ are displacement, velocity, and acceleration for structure (2) respectively, and ks is spring stiffness.

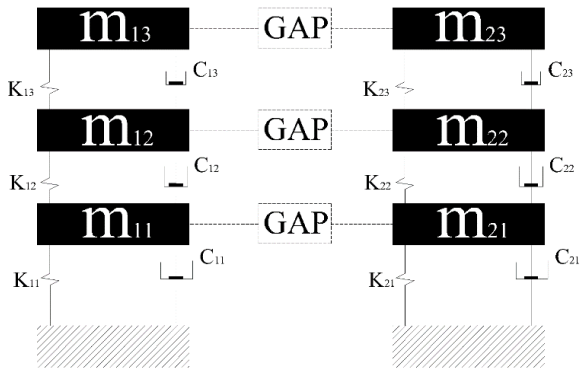

Figure 6 MDOF for two adjacent structures. (Mate, Bakre, and Jaiswal 2015)

2.2 Materials Properties

Table 1 lists key properties of reinforced cement concrete, such as, concrete compressive strength of 28 MPa having a density of 25 kN/m^3, yield stress of steel at 420 MPa, Poisson's ratio of 0.2, elastic modulus at 25,000 MPa, thermal expansion coefficient of 0.00001, and shear modulus of 10,360 MPa.

Table 1 Material Properties of the Structures (BNBC-2020)

Characteristics	Values
Compressive strength of reinforced concrete	28 MPa
Yield Stress of Steel	420 MPa
Poisson's Ratio	0.2
Density of Concrete	25 KN/m^3
Elastic Modulus of Concrete	25000 MPa
Coefficient of Thermal Expansion	0.00001
Shear Modulus	10360

2.3 Properties of the Gap Element

The distance between buildings that are adjacent to each other has been represented by employing a specific gap element that was employed in a nonlinear program, as illustrated in Figure 7. This component is mostly used to transfer compressive pressure; it only becomes active when two buildings come into contact. Crucially, it does not activate under tension or when the relative displacement between neighboring parts is smaller than the distance of the original separation. Two crucial characteristics that define this nonlinear gap element are opening and stiffness. These characteristics are essential for controlling how the element behaves, how it reacts to outside influences, and how well it replicates the dynamic interactions between neighboring components. The values of those two properties (opening and stiffness) have been shown in table 2. This gap element was employed at the interface points of the columns of the structures to measure the pounding forces.

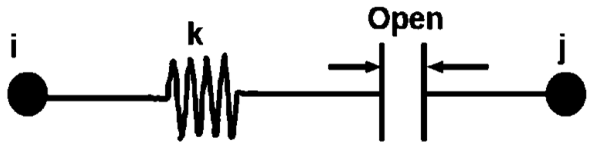

Figure 7 Gap Element (Rajaram and Ramancharla 2014)

Table 2 Properties of the gap element

Property definitions	Values
Stiffness, K (Using Kelvin-Voight method)	2×10^6 KN/m (Maison and Kasai 1992)
Opening or the separation distance between two adjacent structures (Maintaining a short gap between adjacent structures is essential for accurately measuring the pounding force)	5 mm and 10 mm

Although most of the code, such as, Uniform Building Code (ICBO 1997), Bangladesh National Building Code (BNBC-2020), India Standard , International Building Code (ICC 2006) determine the separation gap by referencing the maximum displacement of the neighboring structure. But in this case, the smallest separation distances (5 mm and 10 mm) have been assumed to generate the maximum pounding force of the adjacent structures at nearest distance.

2.4 Vertical Loads

According to Bangladesh National Building Code 2020 (BNBC-2020), there are certain parameters of the applied live loads, partition wall loads and floor finish loads in a structure. The values have been mentioned below in table 3.

Table 3 Vertical Load Patterns (BNBC-2020)

Load Patterns	Values
Live Load	2 KN/m^2
Roof Live Load	4.8 KN/m^2
Partition Wall Load	1.2 KN/m^2
Floor Finish Load	1 KN/m^2

2.5 Seismic Loads

It is necessary to perform a time history analysis to determine the structure's structural reaction and response during as well as after the earthquake excitation. Four seismic records are utilized in this study. The earthquake records of Umbria Marche, Kobe, Imperial Valley, and Chi Chi which had varieties of ground motions. These types of ground motion records have been selected as they all have earthquake magnitudes between 6-8 and they all have PGA (Peak Ground Acceleration) values ranging from low to moderate to high. All these earthquake information and the relative ground motion records have been collected from PEER Ground Motion Database (PEER). The time history function graphs of the related earthquakes have been displayed in Figures 8-11.

(i) Umbria Marche, Italy: The earthquake in Umbria Marche occurred in 1997 and had a magnitude of 6. Its PGA (Peak Ground Acceleration) value was 0.02g.

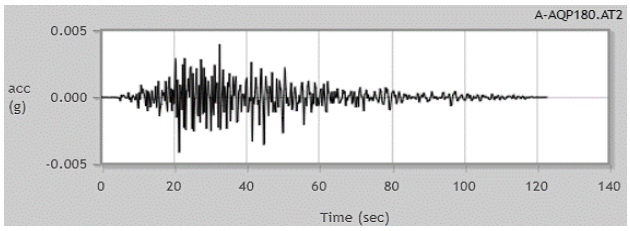

Figure 8 Time history function graph of Umbria Marche earthquake, Italy, 1997.

(ii) Kobe, Japan: In 1995 an earthquake shook Japan with a magnitude of 6.9. This earthquake is known as the Kobe earthquake. It had a PGA value of 1.05g.

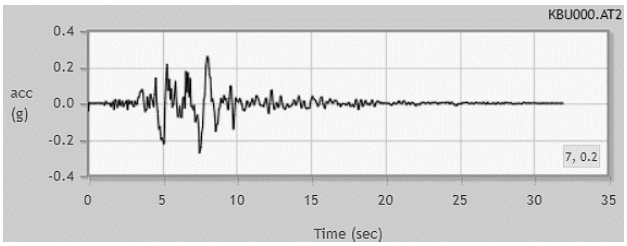

Figure 9 Time history function graph of Kobe earthquake, Japan, 1995.

(iii) Imperial Valley, USA: The Imperial Valley, 1940 earthquake which is also known as the El Centro earthquake had a magnitude of 6.95 and a PGA value of 0.98g.

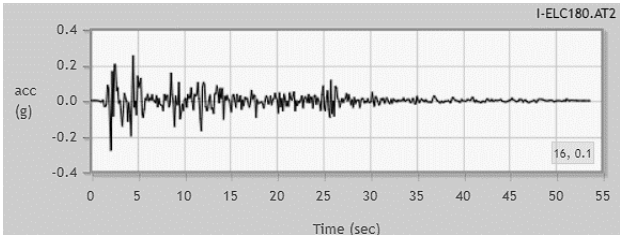

Figure 10 Time history function graph of Imperial Valley earthquake, USA, 1940.

(iv) Chi Chi, Taiwan: In this study, the Chi-Chi earthquake that occurred in Taiwan in 1999, had a maximum magnitude of 7.62. Although it had a PGA value of 0.26g.

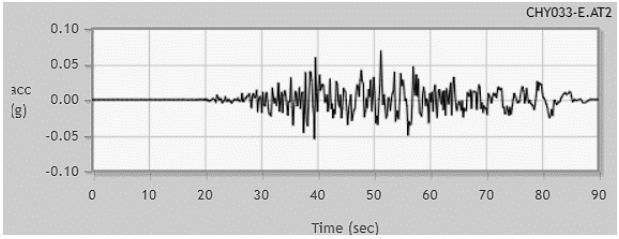

Figure 11 Time history function graph of Chi-Chi earthquake, Taiwan, 1999.

2.6 Components of the Structures

Buildings that have been analyzed were designed according to BNBC 2020 code (BNBC-2020) requirements. Table 4 summarizes the dimensions of the beams and columns of the analyzed structures.

Table 4 Dimensions of the structures

Buildings	Beams	Inner Columns	Outer Columns	Slab Thickness	Floor Height (m)
Smaller Building	12”x18”	14”x16”	16”x18”	5”	10’
Larger Building	12”x18”	15”x18”	16”x20”	6.5”	10’

2.7 Description of the Adjacent Structures

This study includes models of two adjacent structures with different floor levels: initially, low-rise buildings with 7 and 10 floors, and subsequently, high-rise buildings with 12 and 20 floors. To understand the variation of pounding forces due to the increase in floor levels those high-rise and low-rise models have been chosen. Though the models are built following the guidelines of BNBC 2020 code (BNBC-2020) provisions but there are no exact on site structures of those models. Figures 12 and 13 display the plan view layout of the 2 structures separately. Besides, the 3D view has been shown in Figures 14 and 15 so that it becomes easier to understand the elevation differences between two structures.

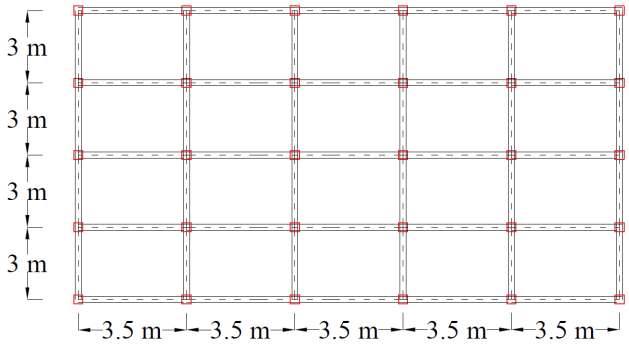

Figure 12 Layout of the smaller structure (Plan View)

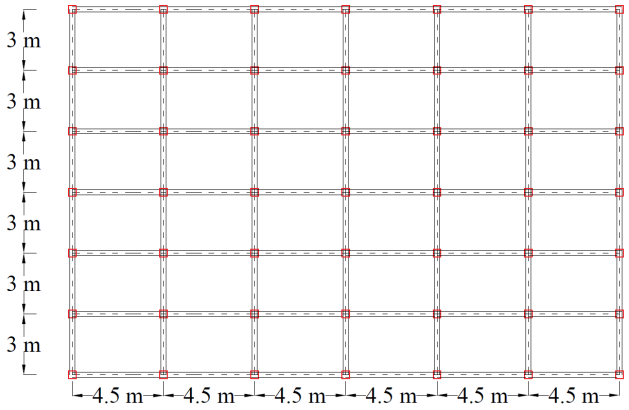

Figure 13 Layout of the larger structure (Plan View).

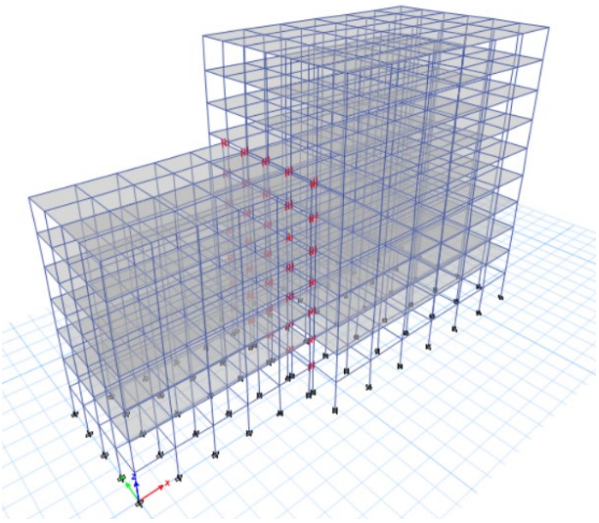

Figure 14 3D view of adjacent low-rise structure.

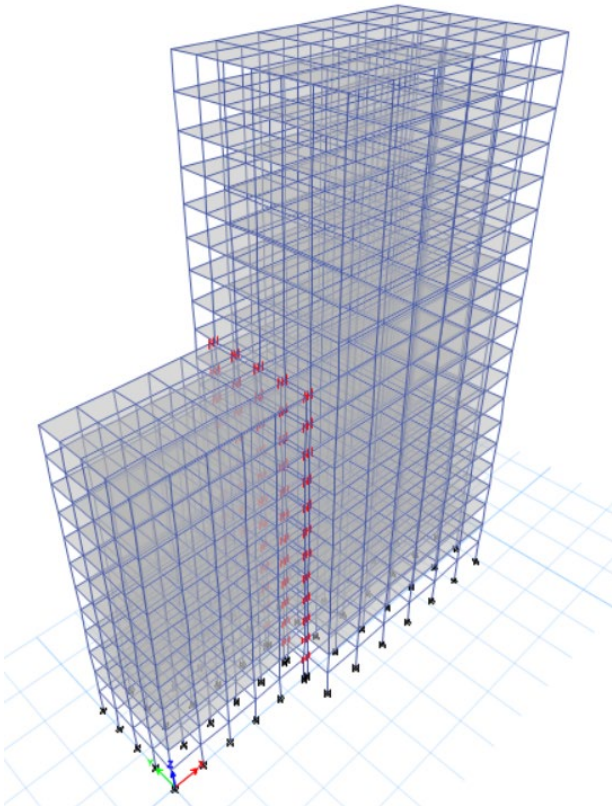

Figure 15 3D view of adjacent high-rise structure.

2.7.1 Low-Rise Adjacent Structures

At first, with the help of the finite element software, two adjacent structures of 7-story and 10-story have been modeled with variations in the elevations. The elevation view of the adjacent structures has been displayed in Figures 16-18.

Model 1:

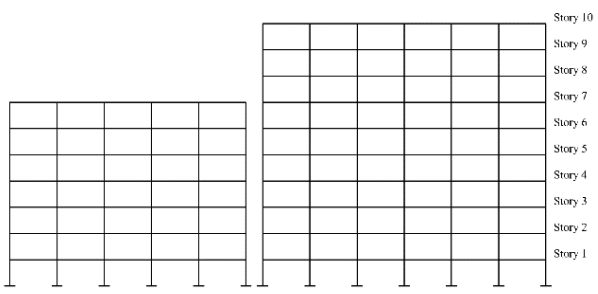

Figure 16 A 7-story building and a 10-story building.

Model 2:

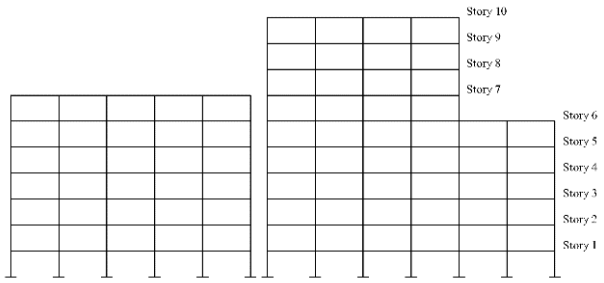

Figure 17 A 7-story building and a vertically irregular 10-story building.

Model 3:

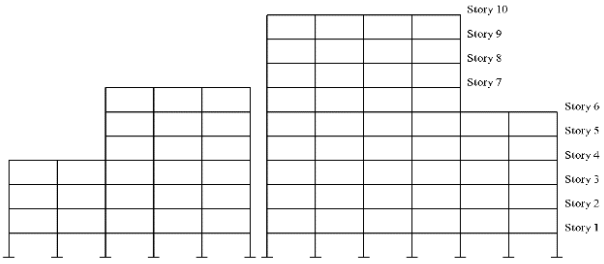

Figure 18 Two irregular 7-story building and 10-story building.

2.7.2 High-Rise Adjacent Structures

After modelling the low-rise structures, there comes a necessity to check the results in the high-rise structures. To analyze that, again two adjacent structures have been modeled of 12 stories and 20 stories adjacently with the help of the finite element software to analyze the results with variations in the elevations. The elevation view of the high-rise adjacent structures has been displayed in Figures 19-21.

Model 4:

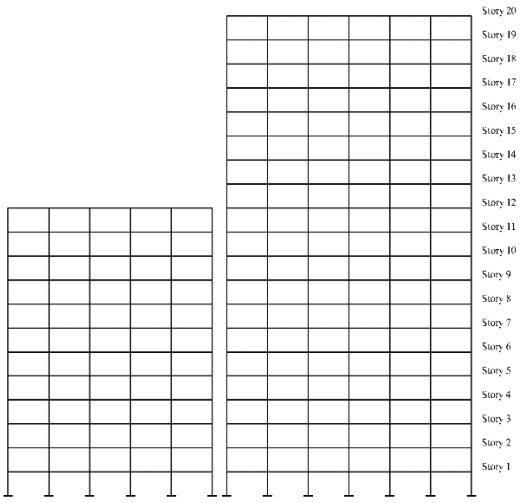

Figure 19 A 12-story building and a 20-story building.

Model 5:

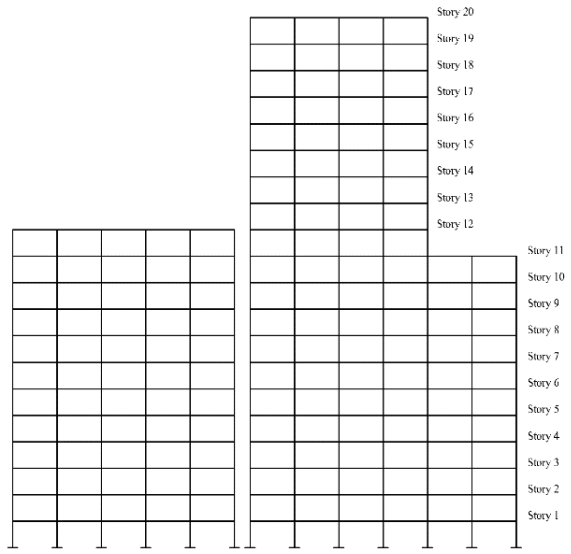

Figure 20 A 12-story building and a vertically irregular 20-story building.

Model 6:

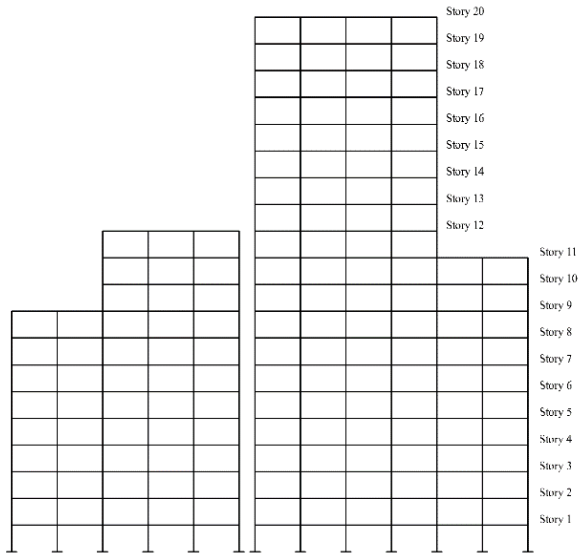

Figure 21 Two irregular 12-story building and 20-story buildings.

3.0 RESULTS AND DISCUSSION

3.1 Maximum Pounding Forces due to different Ground Motions

In this phase, the maximum pounding forces respective to the floor levels due to different ground motions of multiple earthquakes have been discussed. Each of the models have been analyzed in two cases.

(i) Case 1: Pounding forces for the separation distance of 5 mm which have been displayed and discussed in Figures 22-27.

(ii) Case 2: Pounding forces for the separation distance of 10 mm which have been displayed and discussed in Figure 28- 33.

Case 1: Pounding Forces for 5 mm gap distance
Model 1:

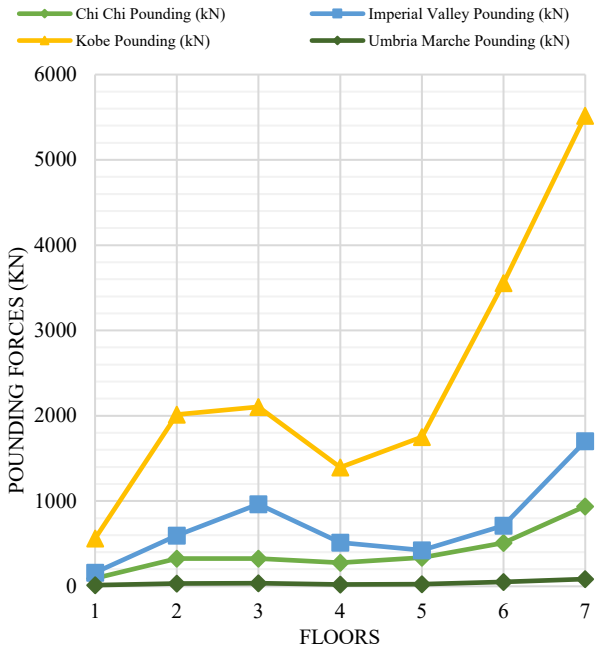

Figure 22 Pounding forces between a 7-story and a 10-story building (5 mm).

In Figure 22, the pounding forces for all the ground motions with respect to floor levels have been plotted. In this case it has been observed that the minimum pounding force between the two adjacent structures for the ground motion of Chi Chi earthquake is 85.1% higher than the pounding force of Umbria Marche earthquake. Again, the min. pounding force values due to the Imperial Valley earthquake is 41.9% greater than that of Chi Chi earthquake. Also, the minimum pounding force of Kobe earthquake is 71.2% greater than that of Imperial Valley earthquake. Analyzing the maximum pounding forces, the value due to Kobe earthquake is 69.2% higher than the value of Imperial Valley earthquake; the maximum value due to Imperial Valley earthquake is 44.8% higher than Chi Chi earthquake; and the maximum value due to Chi Chi earthquake is 90.9% higher than the values of Umbria Marche earthquake. This graph shows a clear view that the maximum pounding force and the minimum pounding force occur at the top floor and first floor respectively. Besides, with the increase in the PGA values the pounding force values increase. This graph shows the decreasing sequence of pounding forces due to the decrease in ground motions of Kobe (1.05g) > Imperial Valley (0.98g) > Chi Chi (0.26g) > Umbria Marche (0.02g).

Model 2:

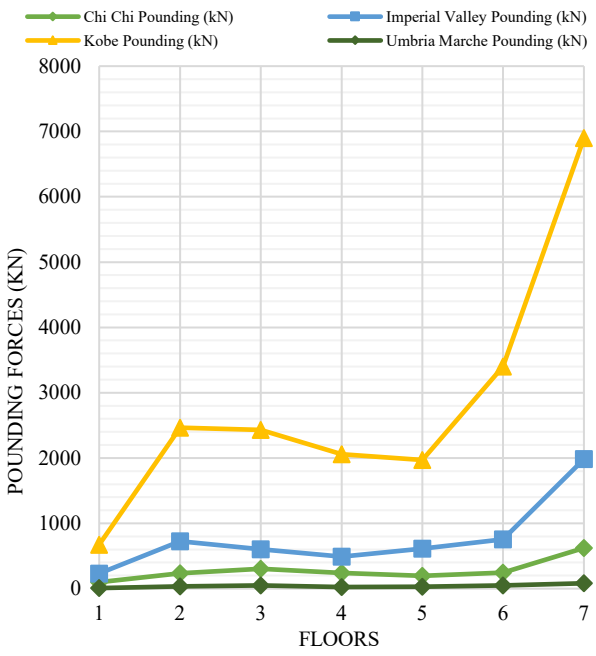

Figure 23 Pounding forces between a 7-story building and a vertically irregular 10-story building (5 mm).

Figure 23 displays pounding forces experienced on different floor levels for the respective earthquakes. In this case it has been observed that, the minimum pounding force between the two adjacent structures for the ground motion of Chi Chi earthquake is 91% higher than the pounding force of Umbria Marche earthquake. Again, the minimum pounding force values due to the Imperial Valley earthquake is 57.4% greater than that of Chi Chi earthquake. Also, the minimum pounding force of Kobe earthquake is 65.5% greater than that of Imperial Valley earthquake. While analyzing the maximum pounding forces, the values of Kobe earthquake is 71.3% higher than the values of Imperial Valley earthquake; the values of Imperial Valley earthquake is 68.6% higher than Chi Chi earthquake; and the values of Chi Chi earthquake is 86.8% higher than the values of Umbria Marche earthquake. This graph also shows the maximum pounding force and the minimum pounding force occur at the top floor and first floor respectively. This phenomenon occurs as the upper floors experience greater lateral displacement during the earthquake which causes higher chances of the increase in pounding force, while lower floors have relatively lesser movement due to their greater structural stiffness. Besides, with the increase in the PGA values the pounding force values increase. This graph shows the decreasing sequence of pounding forces due to the ground motions of Kobe (1.05g) > Imperial Valley (0.98g) > Chi Chi (0.26g) > Umbria Marche (0.02g). Additionally, it can also be observed that, due to consisting of an irregular structure in model 2, there are variations in the pounding forces as well. For Kobe and Imperial Valley earthquake, the maximum pounding forces in model 2 are higher than the pounding force of model 1, where, for Chi Chi and Umbria Marche earthquake, the maximum pounding forces of model 2 are slightly lesser than the model 1 pounding forces.

Model 3:

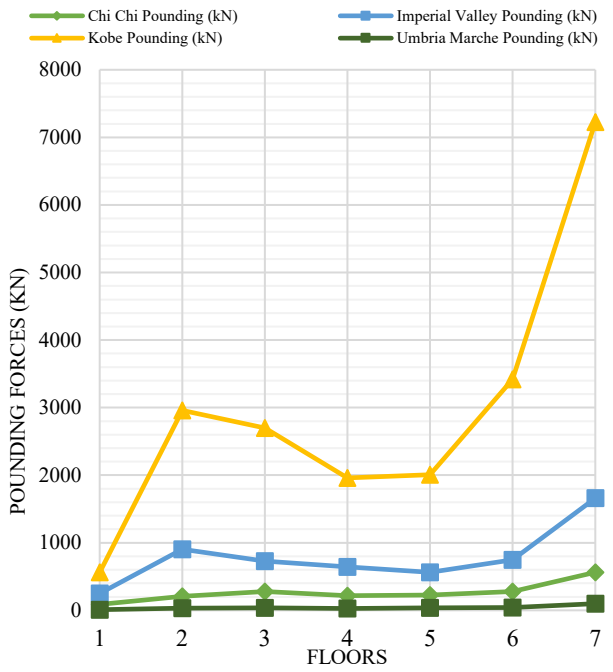

Figure 24 Pounding forces between two irregular 7-story and 10-story building (5 mm).

Figure 24 illustrates the variation of pounding forces at different floor levels for each earthquake. In this case it has been observed that, the minimum pounding force between the two adjacent structures for the ground motion of Chi Chi earthquake is 89.1% higher than the pounding force of Umbria Marche earthquake. Again, the minimum pounding force values due to Imperial Valley earthquake is 64.7% greater than that of Chi Chi earthquake. Also, the min pounding force of Kobe earthquake is 55.6% greater than that of Imperial Valley earthquake. Analyzing the maximum pounding forces, the values of Kobe earthquake is 77% higher than the values of Imperial Valley earthquake; the values of Imperial Valley earthquake is 66.1% higher than Chi Chi earthquake; and the values of Chi Chi earthquake is 82.5% higher than the values of Umbria Marche earthquake. Like before this graph also shows that, the maximum pounding force and the minimum pounding force occur at the top floor and first floor respectively. Besides, with the increase in the PGA values the pounding force values increase. This graph shows the decreasing sequence of pounding forces due to the ground motions of Kobe (1.05g) > Imperial Valley (0.98g) > Chi Chi (0.26g) > Umbria Marche (0.02g). Moreover, consisting of two irregular structures, there comes also variations of pounding forces in model 3 in comparison with model 1. For Kobe and Umbria Marche earthquake, the maximum pounding forces in model 3 are greater than the forces of model 1, where, for Imperial Valley and Chi Chi earthquake, the values of model 3 are smaller than that of model 1 pounding force values.

Model 4:

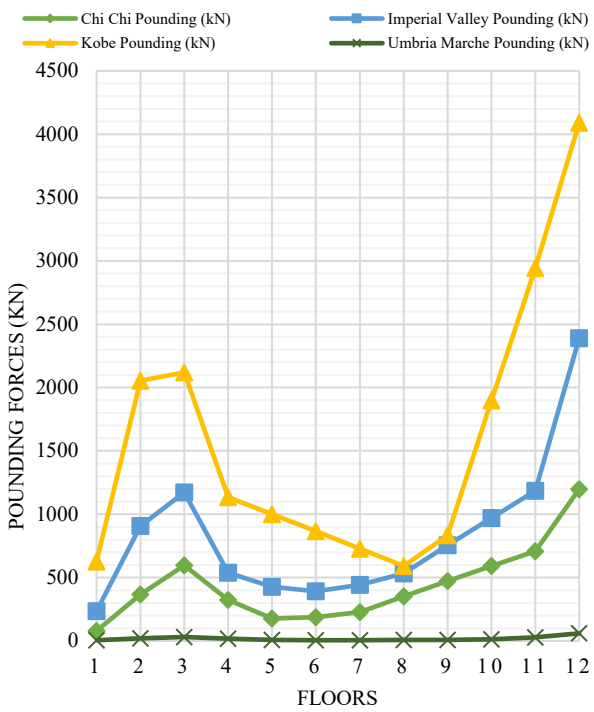

Figure 25 Pounding forces between a 12-story and a 20-story building (5 mm).

In Figure 25, the pounding forces for all the ground motions with respect to floor levels have been plotted. In this case it has been observed that the minimum pounding force between the two adjacent structures for the ground motion of Chi Chi earthquake is 92.7% higher than the pounding force of Umbria Marche earthquake. Again, the minimum pounding force values due to the Imperial Valley earthquake is 66.2% greater than that of Chi Chi earthquake. Also, the minimum pounding force of Kobe earthquake is 62.3% greater than that of Imperial Valley earthquake. While analyzing the maximum pounding forces, the values of Kobe earthquake is 41.6% higher than the values of Imperial Valley earthquake; the values of Imperial Valley earthquake is 49.8% higher than Chi Chi earthquake; and the values of Chi Chi earthquake is 95% higher than the values of Umbria Marche earthquake. In this case, it can also be seen that, the maximum pounding force and the minimum pounding force occur at the top floor and first floor respectively. Besides, with the increase in the PGA values the pounding force values increase. This graph shows the decreasing sequence of pounding forces due to the ground motions of Kobe (1.05g) > Imperial Valley (0.98g) > Chi Chi (0.26g) > Umbria Marche (0.02g). Furthermore, a comparison with Figure 22 (Model 1) reveals that, under the ground motions of the Kobe and Umbria Marche earthquakes, adjacent structures with greater mass (Model 4) experience relatively lower pounding forces than those with smaller mass (Model 1). In contrast, for the Imperial Valley and Chi-Chi earthquakes, the structures with larger mass (Model 4) exhibit relatively higher pounding forces compared to those with smaller mass (Model 1).

Model 5:

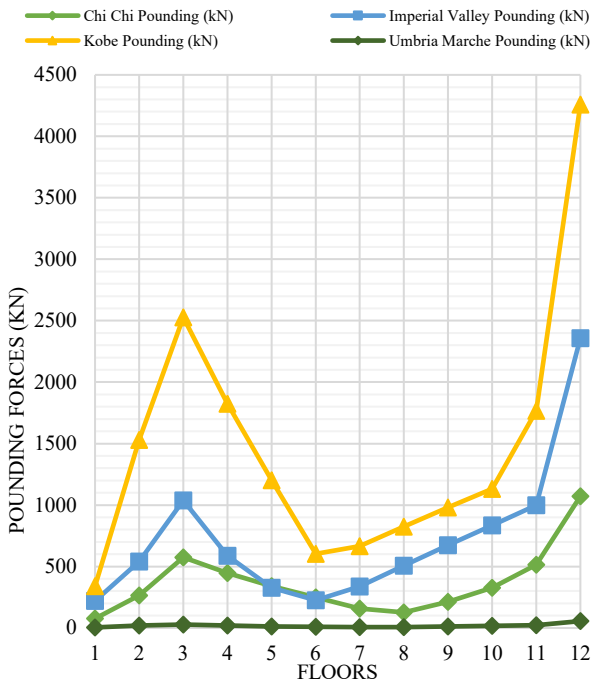

Figure 26 Pounding forces between a 12-story building and a vertically irregular 20-story building (5 mm).

Figure 26 displays pounding forces experienced on the different floor levels for the respective earthquakes. In this case it has been observed that, the minimum pounding force between the two adjacent structures for the ground motion of Chi Chi earthquake is 94% higher than the pounding force of Umbria Marche earthquake. Again, the minimum pounding force values due to Imperial Valley earthquake is 65.4% greater than that of Chi Chi earthquake. Also, the minimum pounding force of Kobe earthquake is 35.4% greater than that of Imperial Valley earthquake. Analyzing the maximum pounding forces, the values of Kobe earthquake is 44.6% higher than the values of Imperial Valley earthquake; the values of Imperial Valley earthquake is 54.5% higher than Chi Chi earthquake; and the values of Chi Chi earthquake is 94.8% higher than the values of Umbria Marche earthquake. Just like the previous graphs, this graph also shows that the maximum pounding force and the minimum pounding force occurs at the top floor and first floor respectively. Besides, with the increase in the PGA values the pounding force values increase. This graph shows the decreasing sequence of pounding forces due to the ground motions of Kobe (1.05g) > Imperial Valley (0.98g) > Chi Chi (0.26g) > Umbria Marche (0.02g). In addition, it can also be observed that, due to consisting of an irregular structure in model 5, similar occurrences like model 2 can also be seen here. For Imperial Valley, Chi Chi and Umbria Marche earthquake, the maximum pounding forces in model 5 are smaller than the pounding force of model 4, where, only for Kobe earthquake, the maximum pounding force of model 5 is slightly higher than the model 4 pounding forces.

Model 6:

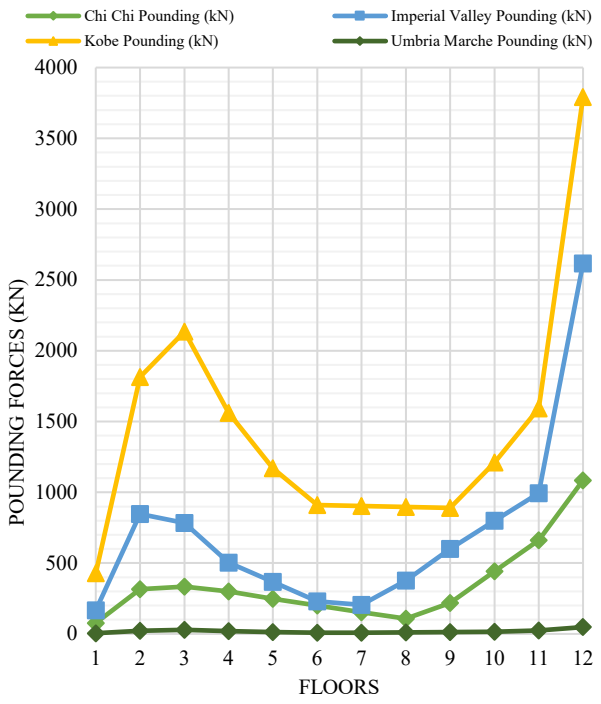

Figure 27 Pounding forces between two irregular 12-story and 20-story building (5 mm).

Figure 27 illustrates the variation of pounding forces at different floor levels for each earthquake. In this case it has been observed that, the minimum pounding force between the two adjacent structures for the ground motion of Chi Chi earthquake is 93.7% higher than the pounding force of Umbria Marche earthquake. Again, the minimum pounding force values due to Imperial Valley earthquake is 54.1% greater than that of Chi Chi earthquake. Also, the minimum pounding force of Kobe earthquake is 60.9% greater than that of Imperial Valley earthquake. While analyzing the maximum pounding forces, the values of Kobe earthquake is 31% higher than the values of Imperial Valley earthquake; the values of Imperial Valley earthquake is 58.6% higher than Chi Chi earthquake; and the values of Chi Chi earthquake is 95.6% higher than the values of Umbria Marche earthquake. From this graph, it can be seen that, the maximum pounding force and the minimum pounding force occurs at the top floor and first floor respectively. Besides, with the increase in the PGA values the pounding force values increase. This graph shows the decreasing sequence of pounding forces due to the ground motions of Kobe (1.05g) > Imperial Valley (0.98g) > Chi Chi (0.26g) > Umbria Marche (0.02g). Moreover, consisting of two irregular structures, a similar phenomenon of model 3 can also be noticed here. For Kobe, Chi Chi and Umbria Marche earthquake, the maximum pounding forces in model 4 are greater than the forces of model 6, where, for Imperial Valley earthquake, the maximum value of model 4 is smaller than that of model 6 pounding force value.

Case 2: Pounding Forces for 10 mm gap distance
Model 1:

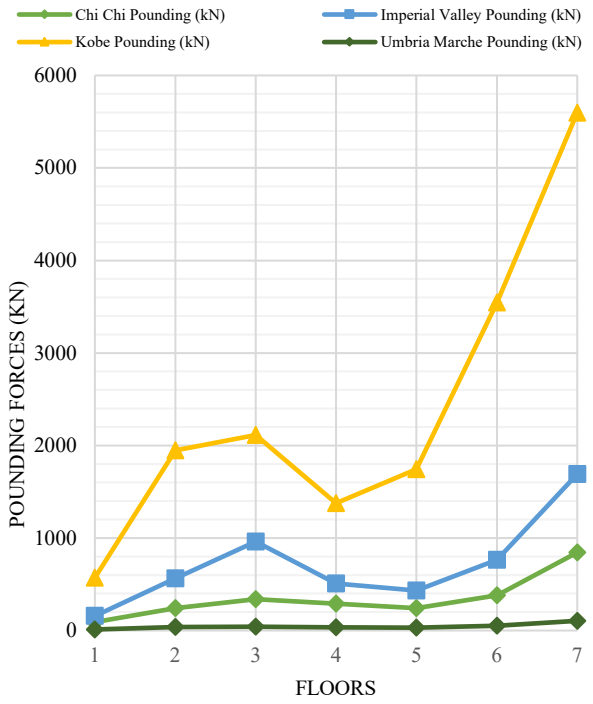

Figure 28 Pounding forces between a 7-story and a 10-story building (10 mm).

In Figure 28, the pounding forces for all the ground motions with respect to floor levels have been plotted. In this case it has been observed that, the minimum pounding force between the two adjacent structures for the ground motion of Chi Chi earthquake is 87.3% higher than the pounding force of Umbria Marche earthquake. Again, the minimum pounding force values due to Imperial Valley earthquake is 41.9% greater than that of Chi Chi earthquake. Also, the minimum pounding force of Kobe earthquake is 72.4% greater than that of Imperial Valley earthquake. Analyzing the maximum pounding forces, the values of Kobe earthquake is 69.8% higher than the values of Imperial Valley earthquake; the values of Imperial Valley earthquake is 50.1% higher than Chi Chi earthquake; and the values of Chi Chi earthquake is 87.6% higher than the values of Umbria Marche earthquake. From this graph, it can be noticed that, the maximum pounding force and the minimum pounding force occurs at the top floor and first floor respectively. Besides, with the increase in the PGA values the pounding force values increase. This graph shows the decreasing sequence of pounding forces due to the ground motions of Kobe (1.05g) > Imperial Valley (0.98g) > Chi Chi (0.26g) > Umbria Marche (0.02g).

Model 2:

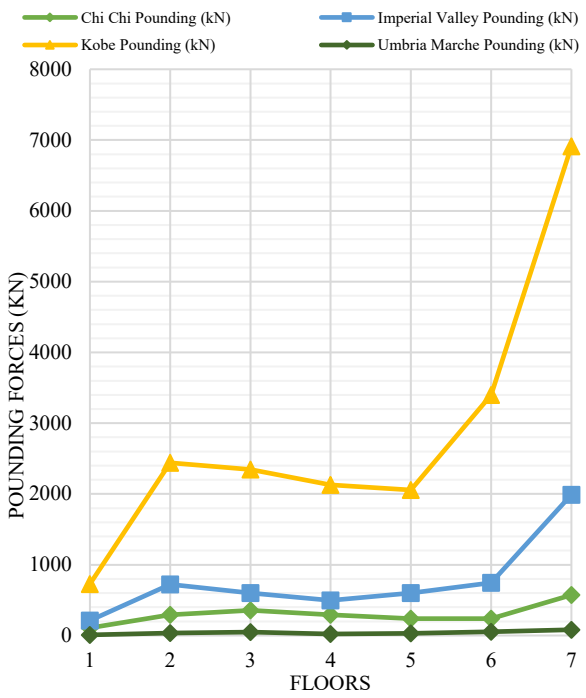

Figure 29 Pounding forces between a 7-story building and a vertically irregular 10-story building (10 mm).

Figure 29 displays pounding forces experienced on the different floor levels for the respective earthquakes. In this case it has been observed that, the minimum pounding force between the two adjacent structures for the ground motion of Chi Chi earthquake is 91.8% higher than the pounding force of Umbria Marche earthquake. Again, the minimum pounding force values due to Imperial Valley earthquake is 49.1% greater than that of Chi Chi earthquake. Also, the minimum pounding force of Kobe earthquake is 70.9% greater than that of Imperial Valley earthquake. While analyzing the maximum pounding forces, the values of Kobe earthquake is 71.2% higher than the values of Imperial Valley earthquake; the values of Imperial Valley earthquake is also 71.2% higher than Chi Chi earthquake; and the values of Chi Chi earthquake is 85.7% higher than the values of Umbria Marche earthquake. The maximum pounding force and the minimum pounding force occurs at the top floor and first floor respectively. Besides, it seems noticeable that, with the increase in the PGA values the pounding force values increase. This graph shows the decreasing sequence of pounding forces due to the ground motions of Kobe (1.05g) > Imperial Valley (0.98g) > Chi Chi (0.26g) > Umbria Marche (0.02g). Additionally, it can also be observed that, due to consisting of an irregular structure in model 2, there are variations in the pounding forces as well. For Kobe and Imperial Valley earthquake, the maximum pounding forces in model 2 are higher than the pounding force of model 1, where, for Chi Chi and Umbria Marche earthquake, the maximum pounding forces of model 2 are slightly lesser than the model 1 pounding forces.

Model 3:

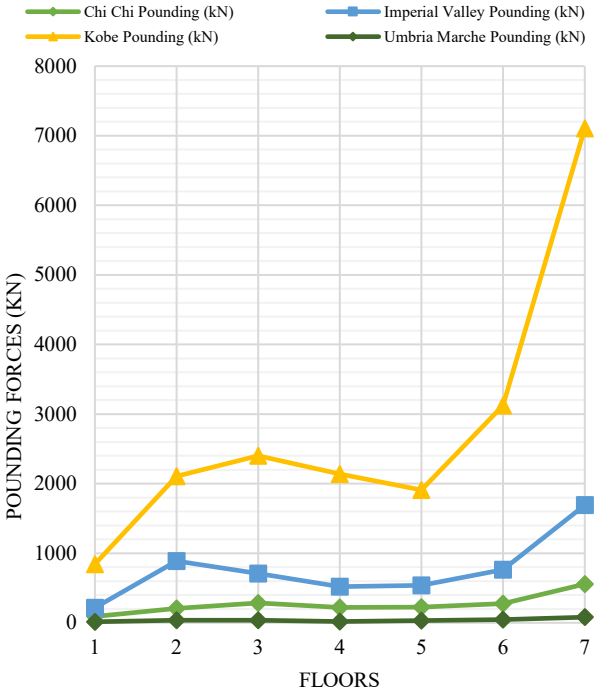

Figure 30 Pounding forces between two irregular 7-story and 10-story building (10 mm).

Figure 30 illustrates the variation of pounding forces at different floor levels for each earthquake. In this case it has been observed that, the minimum pounding force between the two adjacent structures for the ground motion of Chi Chi earthquake is 83.7% higher than the pounding force of Umbria Marche earthquake. Again, the minimum pounding force values due to Imperial Valley earthquake is 58% greater than that of Chi Chi earthquake. Also, the minimum pounding force of Kobe earthquake is 74.3% greater than that of Imperial Valley earthquake. Analyzing the maximum pounding forces, the values of Kobe earthquake is 76.2% higher than the values of Imperial Valley earthquake; the values of Imperial Valley earthquake is 67.1% higher than Chi Chi earthquake; and the values of Chi Chi earthquake is 85.5% higher than the values of Umbria Marche earthquake. The highest pounding force occurs on the top floor, while the lowest pounding force is observed on the first floor. In addition, with the increase in the PGA values the pounding force values increase. This graph shows the decreasing sequence of pounding forces due to the ground motions of Kobe (1.05g) > Imperial Valley (0.98g) > Chi Chi (0.26g) > Umbria Marche (0.02g). Moreover, consisting of two irregular structures, there comes also variations of pounding forces in model 3 in comparison with model 1. For Kobe and Imperial Valley earthquake, the maximum pounding forces in model 3 are greater than the forces of model 1, where, for Chi Chi and Umbria Marche earthquake, the values of model 3 are smaller than that of model 1 pounding force values.

Model 4:

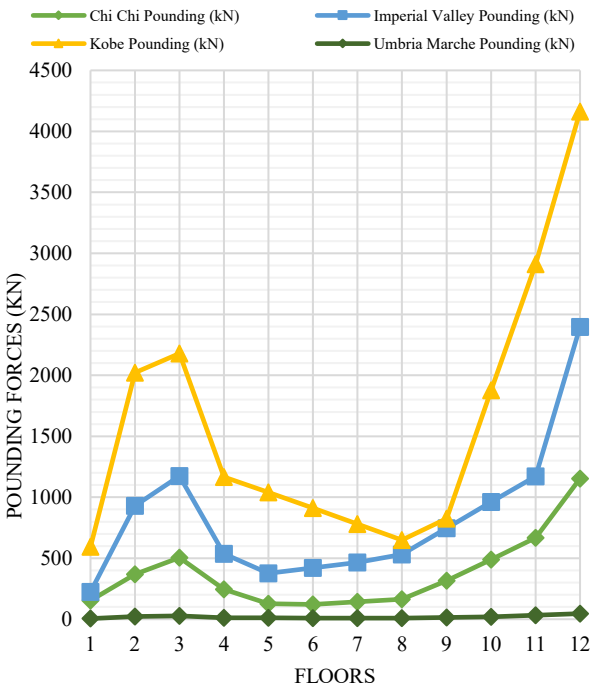

Figure 31 Pounding forces between a 12-story and a 20-story building (10 mm).

In Figure 31, the pounding forces for all the ground motions with respect to floor levels had been shown. In this case it has been observed that, the minimum pounding force between the two adjacent structures for the ground motion of Chi Chi earthquake is 96.5% higher than the pounding force of Umbria Marche earthquake. Again, the minimum pounding force values due to Imperial Valley earthquake is 31.3% greater than that of Chi Chi earthquake. Also, the minimum pounding force of Kobe earthquake is 62.3% greater than that of Imperial Valley earthquake. While analyzing the maximum pounding forces, the values of Kobe earthquake is 42.4% higher than the values of Imperial Valley earthquake; the values of Imperial Valley earthquake is 51.9% higher than Chi Chi earthquake; and the values of Chi Chi earthquake is 96% higher than the values of Umbria Marche earthquake. Here, the greatest pounding force is found on the top floor, whereas the smallest pounding force is on the first floor. Moreover, with the increase in the PGA values the pounding force values increase. This graph shows the decreasing sequence of pounding forces due to the ground motions of Kobe (1.05g) > Imperial Valley (0.98g) > Chi Chi (0.26g) > Umbria Marche (0.02g). Moreover, a similar phenomenon of case 1 can be observed in this case as well. A comparative analysis with the pounding force values shown in Figure 22 (Model 1) indicates that, under the ground motions of the Kobe and Umbria-Marche earthquakes, adjacent structures with greater mass (Model 4) are subjected to comparatively lower pounding forces than those with smaller mass (Model 1). Conversely, for the Imperial Valley and Chi-Chi earthquakes, structures with greater mass (Model 4) experience comparatively higher pounding forces relative to structures with smaller mass (Model 1).

Model 5:

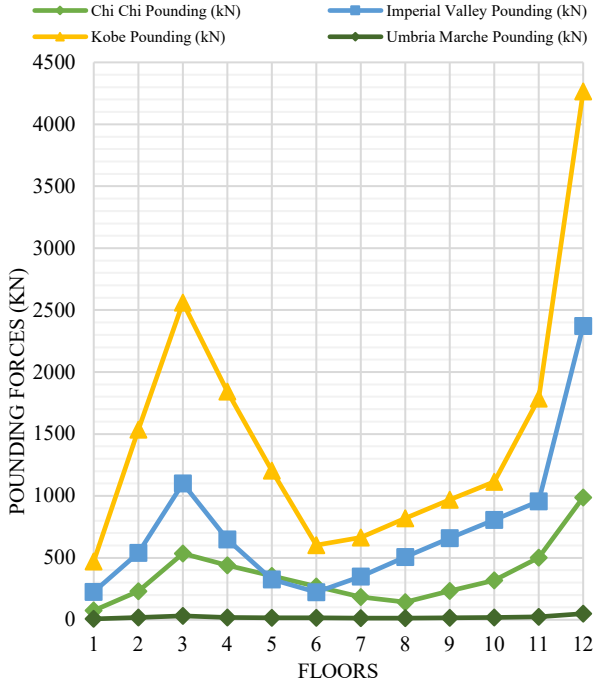

Figure 32 Pounding forces between a 12-story building and a vertically irregular 20-story building (10 mm).

Figure 32 displays pounding forces experienced on the different floor levels for the respective earthquakes. In this case it has been observed that, the minimum pounding force between the two adjacent structures for the ground motion of Chi Chi earthquake is 90.4% higher than the pounding force of Umbria Marche earthquake. Again, the minimum pounding force values due to Imperial Valley earthquake is 67.2% greater than that of Chi Chi earthquake. Also, the minimum pounding force of Kobe earthquake is 52% greater than that of Imperial Valley earthquake. Analyzing the maximum pounding forces, the values of Kobe earthquake is 44.4% higher than the values of Imperial Valley earthquake; the values of Imperial Valley earthquake is 58.3% higher than Chi Chi earthquake; and the values of Chi Chi earthquake is 95% higher than the values of Umbria Marche earthquake. The strongest and weakest pounding forces are felt on the top and bottom floors, respectively. In addition, with the increase in the PGA values the pounding force values also increase. This graph shows the decreasing sequence of pounding forces due to the ground motions of Kobe (1.05g) > Imperial Valley (0.98g) > Chi Chi (0.26g) > Umbria Marche (0.02g). In addition, it can also be observed that, due to consisting of an irregular structure in model 5, similar occurrences like model 2 can also be seen here. For Kobe and Umbria Marche earthquake, the maximum pounding forces in model 5 are higher than the pounding force of model 4, where, for Imperial Valley and Chi Chi earthquake, the maximum pounding force of model 5 is smaller than the model 4 pounding forces.

Model 6:

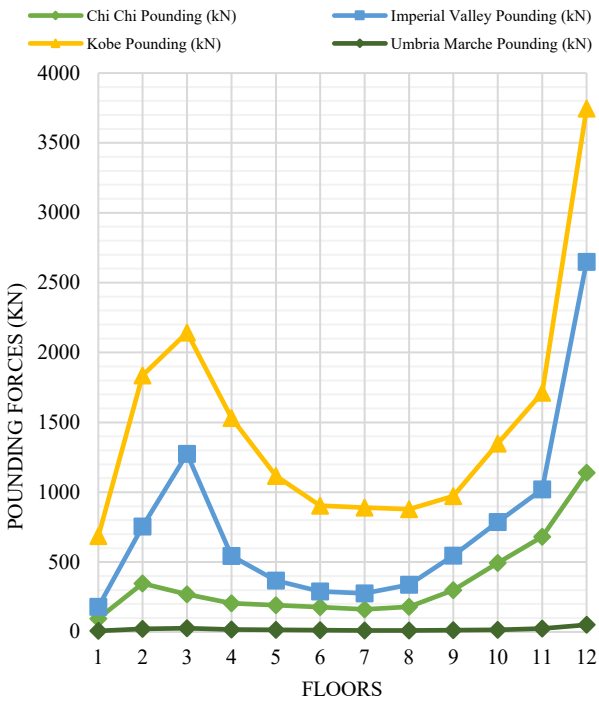

Figure 33 Pounding forces between two irregular 12-story and 20-story building (10 mm).

Figure 33 illustrates the variation of pounding forces at different floor levels for each earthquake. In this case it has been observed that, the minimum pounding force between the two adjacent structures for the ground motion of Chi Chi earthquake is 92.3% higher than the pounding force of Umbria Marche earthquake. Again, the minimum pounding force values due to Imperial Valley earthquake is 46.5% greater than that of Chi Chi earthquake. Also, the minimum pounding force of Kobe earthquake is 73.8% greater than that of Imperial Valley earthquake. While analyzing the maximum pounding forces, the values of Kobe earthquake is 29.3% higher than the values of Imperial Valley earthquake; the values of Imperial Valley earthquake is 57% higher than Chi Chi earthquake; and the values of Chi Chi earthquake is 95.5% higher than the values of Umbria Marche earthquake. The pounding force is at its maximum on the top floor and its minimum on the first floor. Besides, with the increase in the PGA values the pounding force values increase. This graph shows the decreasing sequence of pounding forces due to the ground motions of Kobe (1.05g) > Imperial Valley (0.98g) > Chi Chi (0.26g) > Umbria Marche (0.02g). Moreover, consisting of two irregular structures, a similar phenomenon of model 3 can also be noticed here. For Kobe and Chi Chi earthquake, the maximum pounding forces in model 4 are greater than the forces of model 6, where, for Imperial Valley and Umbria Marche earthquake, the maximum value of model 4 is smaller than that of model 6 pounding force value.

3.2 Effect of Separation/Gap Distance

To acquire the effects of gap/separation distance, the ground motion of Chi-Chi earthquake that occurred in Taiwan in 1999 with a PGA of 0.26g had been chosen due to its highest magnitude of 7.62, had a comparatively mid ranged ground motion as well as stable results in the previous graphs. To attain the results, the pounding forces on each model for gap distance of 5 mm and 10 mm have been analyzed. Here, the bar charts shown in Figure 34-39; the percentage of reduction of the pounding forces of all the models for the separation distances of 5 mm and 10 mm have been displayed.

7-Story and 10-Story building

Model 1:

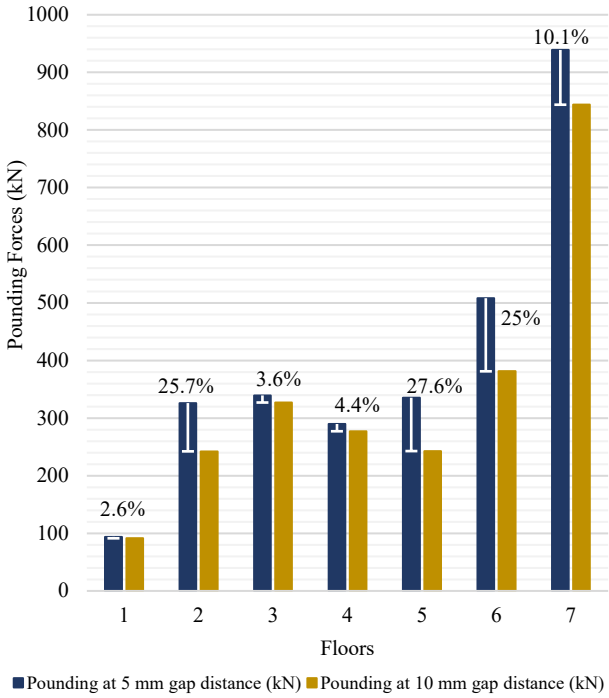

Figure 34 Percentage difference of pounding forces between a 7-story building and a 10-story building for 5 mm and 10 mm separation distance.

Model 2:

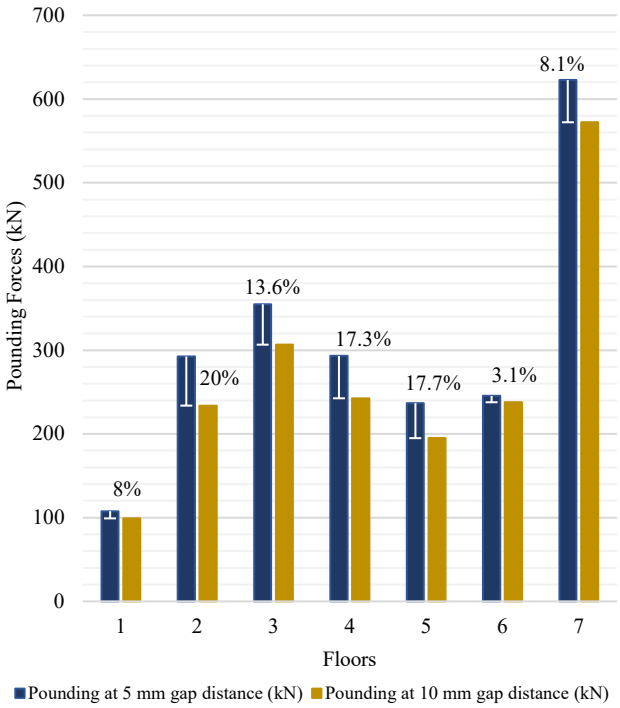

Figure 35 Percentage difference of pounding forces between a 7-story building and a vertically irregular 10-story building for the separation distance of 5 mm and 10 mm.

Model 3:

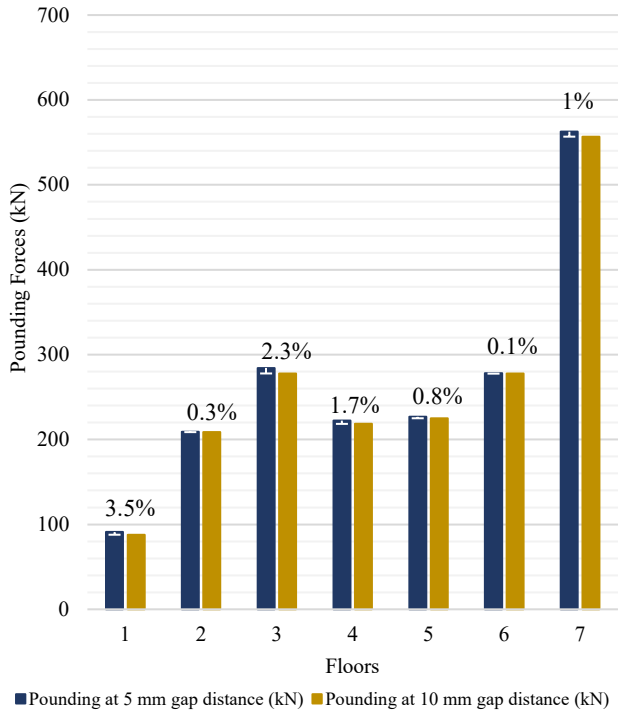

Figure 36 Percentage difference of pounding forces between two irregular 7-story and 10-story buildings for 5 mm and 10 mm separation distance.

12-story and 20-story building

Model 4:

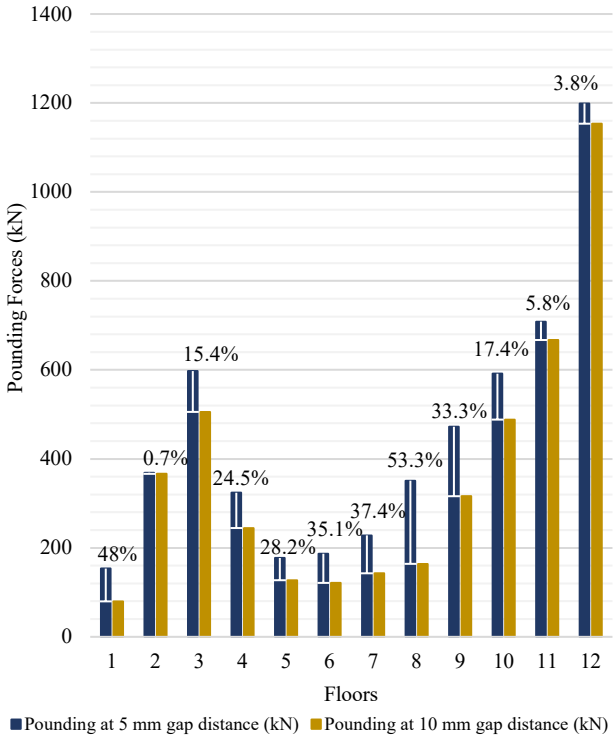

Figure 37 Percentage difference of pounding forces between a 12-story building and a 20-story building for 5 mm and 10 mm separation distance.

Model 5:

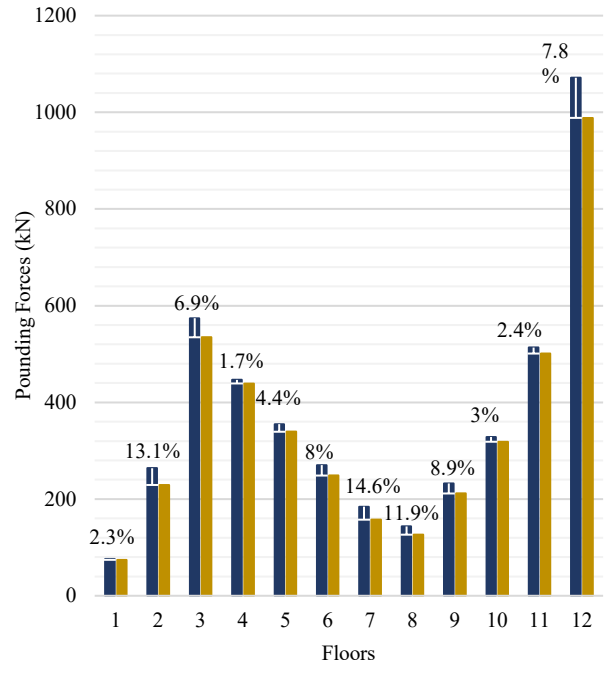

Figure 38 Percentage difference of pounding forces between a 12-story building and a vertically irregular 20-story building for 5 mm and 10 mm separation distance.

Model 6:

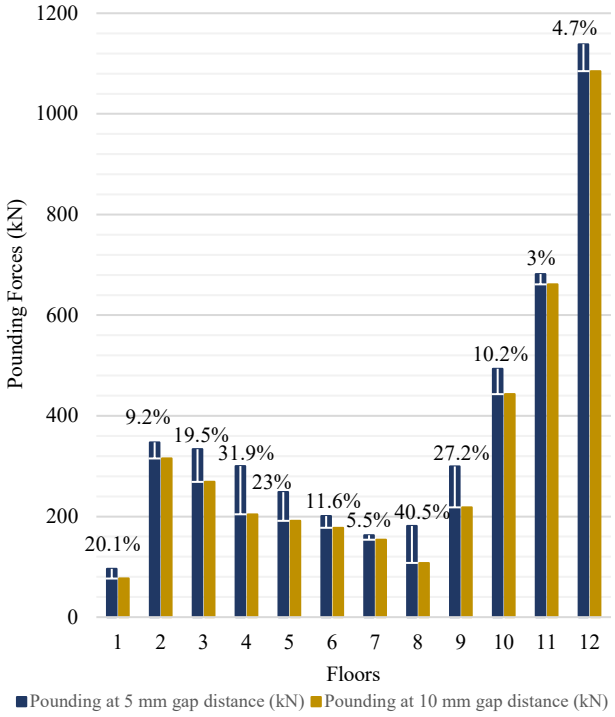

Figure 39 Percentage difference of pounding forces between two irregular 12-story and 20-story buildings for 5 mm and 10 mm separation distance.

The bar charts of this article illustrate the comparison of pounding forces for each floor for the separation distance of 5 mm and 10 mm. Percentages shown in the graphs are the differences of the seismic pounding of the adjacent structures having 5 mm and 10 mm gap distance between them. From the Figures 34-39, it can be concluded that pounding force between adjacent structures gets reduced with the expansion of the gap distance between them.

4.0 CONCLUSION

1) According to subchapter 3.1, it has been clearly visible that the pounding force values at each floor highly depend on the ground acceleration values of the earthquake. With the increase in the values of PGA (Peak Ground Acceleration), the pounding force at each floor gets increased.
2) Separation distance between adjacent structures plays an indispensable role in varying the values of the pounding forces. By increasing the separation distance between the adjacent structures can reduce the pounding force between them. [As per subchapter 3.2]
3) Structural irregularity contributes significantly in differentiating pounding force values. As stated in subchapter 3.1, it can be seen that, the pounding force values change considerably in the irregular structures but do not follow any uniform pattern.
4) Based on subchapters 3.1 and 3.2, by comparing all the graphs, it can be observed that mass of structures also plays a vital role in pounding force. With the change of structural mass as well as ground motion, the pounding forces between the adjacent structures shows considerable variation and do not represent similar patterns in every case.

Acknowledgements

The authors sincerely thank Ahsanullah University of Science and Technology for providing research facilities. Gratitude is also extended to co-authors for their substantial support and contributions, which were indispensable to complete the research. Furthermore, the authors appreciate the anonymous reviewers for their valuable critiques and recommendations, which improved the manuscript.

Conflicts of Interest

The author(s) declare(s) that there is no conflict of interest regarding the publication of this paper

References

[1] Abdel Raheem, Shehata E. 2014. 'Mitigation measures for earthquake induced pounding effects on seismic performance of adjacent buildings', *Bulletin of earthquake engineering*, 12: 1705-24.
[2] Abdel Raheem, Shehata E, Momen MM Ahmed, Mohamed M Ahmed, and Aly GA Abdel-shafy. 2018. 'Evaluation of plan configuration irregularity effects on seismic response demands of L-shaped MRF buildings', *Bulletin of earthquake engineering*, 16: 3845-69.
[3] Abdel Raheem, Shehata E, and T Hayashikawa. 2013. "Mitigation measures for expansion joint effects on seismic performance of bridge structures." In Proceedings of the Thirteenth East Asia-Pacific Conference on Structural Engineering and Construction (EASEC-13), B-1-1. The Thirteenth East Asia-Pacific Conference on Structural Engineering and Construction (EASEC-13).
[4] Anagnostopoulos, Stavros A. 1988. 'Pounding of buildings in series during earthquakes', *Earthquake engineering & structural dynamics*, 16: 443-56.
[5] Anagnostopoulos, Stavros A, and Konstantinos V Spiliopoulos. 1992. 'An investigation of earthquake induced pounding between adjacent buildings', *Earthquake engineering & structural dynamics*, 21: 289-302.
[6] BNBC-2020. '*Bangladesh National Building Code-2020*', Housing and Building Research Institute, Bangladesh.
[7] Cole, Gregory L, Rajesh P Dhakal, and Fred M Turner. 2012. 'Building pounding damage observed in the 2011 Christchurch earthquake', *Earthquake engineering & structural dynamics*, 41: 893-913.
[8] Favvata, Maria J. 2017. 'Minimum required separation gap for adjacent RC frames with potential inter-story seismic pounding', *Engineering structures*, 152: 643-59.
[9] Ghosh, Aparna, and Aviral Kumar. 2023. 'Seismic Induced Pounding of Structures and Its Mitigation.' in T. G. Sitharam, Sreevalsa Kolathayar, Ravi S. Jakka and Vasant Matsagar (eds.), *Theory and Practice in Earthquake Engineering and Technology* (Springer Nature Singapore: Singapore).
[10] Goldsmith, Werner. 1999. *The theory and physical behaviour of colliding solids* (Dover Publ.).
[11] ICBO, T. 1997. "Uniform building code." In *International conference of building officials. Whittier (CA): ICBO*.
[12] ICC. 2006. "International building code 2006." In.: International Code Council Falls Church, Virginia, USA.
[13] Jankowski, Robert. 2009. 'Non-linear FEM analysis of earthquake-induced pounding between the main building and the stairway tower of the Olive View Hospital', *Engineering structures*, 31: 1851-64.
[14] Jankowski, Robert. 2010. 'Experimental study on earthquake-induced pounding between structural elements made of different building

materials', *Earthquake Engineering & Structural Dynamics*, 39: 343-54."

[15] Jeng, V, and WL Tzeng. 2000. 'Assessment of seismic pounding hazard for Taipei City', *Engineering structures*, 22: 459-71.

[16] Kamel, Kamel T. 2023. 'Estimating the seismic pounding force between adjacent buildings and study the effect of gap distance on seismic pounding', *Asian Journal of Civil Engineering*, 24: 153-67.

[17] Kasai, Kazuhiko, and Bruce F Maison. 1997. 'Building pounding damage during the 1989 Loma Prieta earthquake', *Engineering structures*, 19: 195-207.

[18] Kazemi, F, Mahmoud Miari, and Robert Jankowski. 2021. 'Investigating the effects of structural pounding on the seismic performance of adjacent RC and steel MRFs', *Bulletin of earthquake engineering*, 19: 317-43.

[19] Maison, Bruce F, and Kazuhiko Kasai. 1990. 'Analysis for a type of structural pounding', *Journal of Structural Engineering*, 116: 957-77.

[20] Maison, Bruce F, and Kazuhiko Kasai. 1992. 'Dynamics of pounding when two buildings collide', *Earthquake Engineering & Structural Dynamics,* 21: 771-86.

[21] Mate, Nilesh U, SV Bakre, and OR Jaiswal. 2015. 'Seismic pounding of adjacent linear elastic buildings with various contact mechanisms for impact simulation'.

[22] Meli, R, and E Rosenblueth. 1986. 'The 1985 Earthquake causes and effects in Mexico City', *Concrete International, ACI, Detroit, Mich*, 8: 12.

[23] Papadrakakis, Manolis, and Harris P Mouzakis. 1995. 'Earthquake simulator testing of pounding between adjacent buildings', *Earthquake engineering & structural dynamics*, 24: 811-34.

[24] Patil, Basanagouda I, Bapugouda B Biradar, and Rashmi Doddamani. 2022. "Mitigation of seismic pounding observed in adjacent buildings with fluid viscous damper." In *Sustainability Trends and Challenges in Civil Engineering: Select Proceedings of CTCS 2020*, 711-31. Springer.

[25] PEER. 2013. Pacific Earthquake Engineering Research Center. 'PEER Ground Motion Database'. https://ngawest2.berkeley.edu/.

[26] Raheem, SE Abdel. 2013a. 'Mitigation measures for seismic pounding effects on adjacent buildings responses', *Computational Methods in Structural Dynamics and Earthquake Engineering*, 12: 1705-24.

[27] Raheem, Shehata E Abdel. 2006. 'Seismic pounding between adjacent building structures', *Electronic Journal of Structural Engineering*, 6: 66-74.

[28] Raheem, Shehata E Abdel. 2009. 'Pounding mitigation and unseating prevention at expansion joints of isolated multi-span bridges', *Engineering structures,* 31: 2345-56

[29] Raheem, Shehata E Abdel. 2013b. 'Evaluation and mitigation of earthquake induced pounding effects on adjacent buildings performance', *Proceedings of Advances in structural engineering and mechanics (ASEM13),* Jeju, Korea: 8-12."

[30] Rai, Durgesh C, Vaibhav Singhal, Bhushan Raj S, and S Lalit Sagar. 2016. 'Reconnaissance of the effects of the M7. 8 Gorkha (Nepal) earthquake of April 25, 2015', *Geomatics, Natural Hazards and Risk*, 7: 1-17.

[31] Rajaram, Chenna, and Pradeep Kumar Ramancharla. 2014. 'Three dimensional analysis of pounding between adjacent buildings', *Journal of Structural Engineering*, 41: 1-11.